# Myosin Va and microtubule-based motors are required for fast axonal retrograde transport of tetanus toxin in motor neurons

**Giovanna Lalli[1,*], Stephen Gschmeissner[2] and Giampietro Schiavo[1,‡]**

[1]Molecular NeuroPathoBiology Laboratory, and [2]Electron Microscopy Unit, Cancer Research UK, London Research Institute, Lincoln's Inn Fields Laboratories, 44 Lincoln's Inn Fields, London WC2A 3PX, UK

*Present address: MRC Laboratory for Molecular Cell Biology, University College London, Gower Street, London WC1E 6BT, UK

‡Author for correspondence (e-mail: giampietro.schiavo@cancer.org.uk)

*Accepted 27 June 2003*
*Journal of Cell Science 116, 4639-4650 © 2003 The Company of Biologists Ltd*
*doi:10.1242/jcs.00727*

## Summary

**Using a novel assay based on the sorting and transport of a fluorescent fragment of tetanus toxin, we have investigated the cytoskeletal and motor requirements of axonal retrograde transport in living mammalian motor neurons. This essential process ensures the movement of neurotrophins and organelles from the periphery to the cell body and is crucial for neuronal survival. Unlike what is observed in sympathetic neurons, fast retrograde transport in motor neurons requires not only intact microtubules, but also actin microfilaments. Here, we show that the movement of tetanus toxin-containing carriers relies on the nonredundant activities of dynein as well as kinesin family members. Quantitative kinetic analysis indicates a role for dynein as the main motor of these carriers. Moreover, this approach suggests the involvement of myosin(s) in retrograde movement. Immunofluorescence screening with isoform-specific myosin antibodies reveals colocalization of tetanus toxin-containing retrograde carriers with myosin Va. Motor neurons from homozygous myosin Va null mice showed slower retrograde transport compared with wild-type cells, establishing a unique role for myosin Va in this process. On the basis of our findings, we propose that coordination of myosin Va and microtubule-dependent motors is required for fast axonal retrograde transport in motor neurons.**

Movies available online

Key words: Axonal transport, Motor neuron, Myosin Va, Neuronal cytoskeleton, Tetanus toxin

## Introduction

Neuronal homeostasis relies on an efficient bidirectional transport system for the correct and timely targeting of cargoes to distant cellular domains. Axonal anterograde transport allows the delivery of newly synthesized proteins, RNA and other membranous and nonmembranous structures from the cell body to distal neuronal sites (Nakata et al., 1998; Goldstein and Yang, 2000; Brown, 2003). Retrograde transport is essential for organelles and ligands to reach the soma from nerve terminals and perform their biological functions (Goldstein and Yang, 2000; Ginty and Segal, 2002; Brown, 2003). Moreover, virulence factors and pathogens, including tetanus toxin (TeNT) and several neurotropic viruses, exploit this transport route to enter the central nervous system (Schiavo et al., 2000; Tomishima et al., 2001; Butowt and Von Bartheld, 2003).

Multiple motors have been associated with axonal transport. Biochemical, pharmacological and genetic approaches identified dynein as the major microtubule (MT)-based motor responsible for driving retrograde transport in neurons (Schnapp and Reese, 1989; Waterman-Storer et al., 1997; Goldstein and Yang, 2000; Vale, 2003). Additionally, minus-end-directed kinesins such as KIFC2 have been linked to retrograde transport, although functional evidence is still lacking (Hirokawa, 1998; Goldstein and Yang, 2000). Actin cytoskeleton and myosin motors have also been implicated in bidirectional axonal transport (Kuznetsov et al., 1992; Bearer et al., 1993). In squid axoplasm, endoplasmic reticulum-derived vesicles containing both myosin and kinesin move on actin filaments (Tabb et al., 1998). Moreover, axoplasmic organelles and mitochondria are transported on both F-actin and MTs (Kuznetsov et al., 1992; Bearer et al., 1993; Morris and Hollenbeck, 1995). These results point to the presence of both actin- and MT-based motors on the same organelle (Brown, 1999). This concept has been strengthened by work in other systems, such as *Xenopus* melanophores, in which melanosomes are transported bidirectionally on MTs and are dispersed throughout the cytoplasm by myosin V (Rogers and Gelfand, 2000; Langford, 2002; Gross et al., 2002a). Interestingly, myosin V has been shown to interact directly with conventional kinesin, indicating that MT- and actin-based motors could exist in multifunctional complexes transporting organelles along both cytoskeletal systems in a coordinated fashion (Huang et al., 1999; Langford, 2002).

These observations support a 'dual filament' model of transport (Langford, 1995; Langford, 2002), predicting a functional cooperation between MTs and the actin cytoskeleton. MT-based motors would ensure long-range transport, whereas myosins could allow local movement of organelles on F-actin in areas devoid of MT as, for example,

nerve terminals, growth cones and subcortical plasma membrane regions. Probable candidates for powering such short-range movements are unconventional myosins, such as Va, VI and VII (DePina and Langford, 1999; Wu et al., 2000). However, with the notable exception of myosin V, little is know about the localization and function of unconventional myosins and their role in axonal transport (Bridgman and Elkin, 2000). By contrast, myosin Va has been investigated in detail and is found associated with different nonmembranous cargoes, such as neurofilament NF-L subunit (Rao et al., 2002) and membrane-enclosed organelles. These include melanosomes (Rogers and Gelfand, 1998), endoplasmic reticulum (Tabb et al., 1998; Wöllert et al., 2002), synaptic vesicles (Prekeris and Terrian, 1997), secretory granules (Neco et al., 2002; Rose et al., 2003) and other axonal vesicles (Evans et al., 1998; Bridgman, 1999). Moreover, myosin V-driven motility of distinct organelles is differentially controlled during the cell cycle (Wöllert et al., 2002).

Despite the importance of axonal retrograde transport in neuronal physiology and disease, few studies have focused on the identification of the machinery responsible for this process in mammalian neurons. Furthermore, the direct visualization of retrograde transport and its quantitative analysis have been hampered by the lack of a reliable assay in living cells. We have recently established such an assay in motor neurons (MNs) by using a nontoxic fluorescent fragment of tetanus toxin (TeNT $H_C$) (Lalli and Schiavo, 2002). TeNT $H_C$ binds with high affinity to mammalian MNs and colocalizes in nonacidic compartments with p75 neurotrophin receptor ($p75^{NTR}$) (Herreros et al., 2001; Lalli and Schiavo, 2002). $p75^{NTR}$ undergoes retrograde axonal transport and is important for targeting neurotrophins to the central nervous system (Butowt and Von Bartheld, 2003). Because TeNT $H_C$ shares a retrograde route with $p75^{NTR}$, it provides an ideal probe for studying this important transport process.

In the present paper, we investigate the cytoskeletal requirements and the identity of the molecular motors involved in the axonal transport of TeNT $H_C$ carriers. Kinetic analysis of this compartment shows that fast retrograde transport in MNs requires both MT- and actin-based motors. Our results suggest that dynein acts not only as a major retrograde motor but also as a coordinator of other MT-based motors. Furthermore, we find that MNs from myosin Va null mice display a slower, more discontinuous TeNT $H_C$ transport compared with wild-type cells, implying that myosin Va is necessary to ensure fast axonal retrograde transport in mammalian MNs.

## Materials and Methods

All reagents were obtained from Sigma, unless otherwise specified. Alexa™ Fluor 488, 546, 594 maleimides, Alexa™ Fluor 488 phalloidin and Texas Red-conjugated goat anti-mouse and anti-rabbit secondary antibodies were from Molecular Probes. Monoclonal anti-β-tubulin antibody was from Roche Diagnostics. A polyclonal rabbit antiserum against rat myosin Va tail (aminoacids 1005-1830) (Evans et al., 1997) was a kind gift from P. C. Bridgman (Washington University School of Medicine, St Louis, MO).

### Preparation and fluorescent labelling of recombinant TeNT $H_C$

Phosphorylated oligonucleotides (5′-GAT CCG CAG AGG CAG CAG CAC GAG AGG CTT GTT GTC GAG AGT GTT GTG CAC GAG AGG CAG CAG CAC GAG CG-3′ and 5′-AAT TCG CTC GTG CTG CTG CCT CTC GTG CAC AAC ACT CTC GAC AAC AAG CCT CTC GTG CTG CTG CCT CTG CG-3′) were annealed and then ligated into the *Bam*HI/*Eco*RI site of pGEX-4T3 (Amersham Pharmacia Biotech), resulting in the pGEX-4T3-Cys vector. TeNT $H_C$ was excised with *Sal*I/*Eco*RI from the pGEX-6 vector (Lalli et al., 1999) and ligated into pGEX-4T3-Cys. The resulting plasmid (pGEX-4T3-Cys-TeNT $H_C$) encodes glutathione *S*-transferase, which is fused to the peptide A EAAAR EACCR ECCAR EAAAR A and to TeNT $H_C$ (Fig. 1A). The boxed domains are predicted to form α-helices with the thiol groups properly oriented for labelling with fluorescein arsenical helix binder (FLASH) (Griffin et al., 1998). TeNT $H_C$ was purified following standard procedure (Lalli et al., 1999), concentrated through dialysis against 10 mM Hepes-NaOH, pH 7.4, 150 mM NaCl, 15% polyethylene glycol 20,000, 5 mM 2-mercaptoethanol and dialysed overnight against 20 mM Hepes-NaOH pH 7.4, 100 mM NaCl, 10% glycerol, 0.1 mM 2-mercaptoethanol.

Before labelling with FLASH, TeNT $H_C$ (1 nanomole) was reduced with 12.5 mM 2-mercaptoethanol for 30 minutes at 37°C. The labelling reaction was performed using 5 nmoles of FLASH-1,2-ethandithiol (Aurora Biosciences) and carried out for 90 minutes at room temperature in the dark. Labelling with the Alexa maleimides was performed according to the manufacturer's instructions.

### Retrograde transport assay in living rodent MNs

Rat spinal cord MNs were purified from E14 Sprague-Dawley embryos and maintained in culture as previously described (Henderson et al., 1995). One week after plating, rat MNs were incubated with 40 nM TeNT $H_C$-Alexa488 (unless otherwise indicated) in Neurobasal medium (GIBCO BRL) at 37°C for 25 minutes, washed and imaged after 20 minutes at 37°C with time-lapse low-light microscopy (Lalli and Schiavo, 2002), using an exposure time of 0.3 seconds for each frame. In competition experiments, MNs were pre-incubated at 37°C for 10 minutes with a 100× excess of native TeNT before adding the fluorescent TeNT $H_C$.

Single embryo cultures enriched in spinal cord MNs were obtained by trypsinization of E13 ventral spinal cords of wild-type mice and mice homozygous for the *dilute lethal* mutation $Myo5a^{d-l}$ (strain DLS/Le a/a $Myo5a^{d-l}$ +/+ $Bmp5^{se}$; Jackson Laboratories, Bar Harbor, ME) (Mercer et al., 1991). Cells were maintained in culture as described (Arce et al., 1999) and used one week after plating. Phenotyping of *dilute lethal* embryos was performed by western blot analysis of brain homogenates as previously described (Evans et al., 1997).

### Drug treatments

Twenty minutes after removing the fluorescent TeNT $H_C$, MNs were incubated at 37°C with 0.5 μM latrunculin B [Lat B, Calbiochem; 1 mM stock in dimethylsulfoxyde (DMSO)] or 5 μM vincristine (Vin; 2 mM stock in methanol). Imaging was resumed 15 minutes after the addition of Lat B or 40 minutes after the addition of Vin. In control MNs, an equal amount of DMSO or methanol (final concentration 0.3% or less) was added and imaging was performed at similar timepoints used for the drug-treated samples. Cells were then fixed and stained for MTs and F-actin (see below).

In other sets of experiments, MNs were incubated with 40 nM TeNT $H_C$-Alexa488 for 25 minutes at 37°C, washed and incubated with the following drugs after 20 minutes: 1 mM erythro-9-(2-hydroxy-3-nonyl)adenine (EHNA; from Calbiochem, 250 mM stock in water), 10 μM aurintricarboxylic acid (AA; 10 mM stock in DMSO) alone or in combination. Imaging resumed 15 minutes after addition of the drugs and stopped before any noticeable change in the morphology of cell bodies or the appearance of neurite blebbing.

### Tracking and data quantification

Vesicle tracking was performed on time-lapse sequences using the Motion Analysis software (Kinetic Imaging) as previously described (Lalli and Schiavo, 2002). Speed and average speed values were determined by measuring the distance covered by each carrier between two consecutive frames or between the initial and the final tracking points, respectively. The speed distributions of TeNT $H_C$ alone or on treatment with motor inhibitors were analysed with KaleidaGraph (Synergy Software) by applying a multiple Gaussian curve fit. Preliminary analysis with unimodal and bimodal Gaussian profiles failed to satisfactorily describe the speed distributions of control and untreated samples. Optimal fitting was obtained by using the sum of three Gaussian profiles centred at the following speeds: for rat, 0, 0.53 and 1.15 μm/second; for mouse, 0, 0.53 and 0.95 μm/second. Datasets with a correlation coefficient $R^2$<0.8 were excluded from the final analysis. The contribution of single speed components was obtained by calculating the integral of the corresponding Gaussian equation in the range of speeds determined experimentally. Each contribution was expressed as a percentage of the sum of the components. The incidence of reversal was calculated by dividing the number of changes of direction (over a distance larger than 0.2 μm) by the number of organelles analysed. Statistical analysis was performed using SigmaPlot 2000 (SPSS Science) and KaleidaGraph. 8-bit images were assembled into movies with the Kinetic Imaging software using the Microsoft Video 1, 100% quality compression algorithm.

### Electron microscopy

Cells were cooled to 4°C, washed twice with 0.2% bovine serum albumin (BSA) in Hanks' buffer (Lalli et al., 1999) and incubated with 10 nm gold-conjugated TeNT $H_C$ (Aurion). After washing three times with 0.2% BSA in Hanks' buffer, cells were either fixed or warmed to 37°C for 5 or 20 minutes before fixing for 1 hour with 2.5% glutaraldehyde in 0.1 M sodium phosphate buffer, pH 7.4 (Sorensen's buffer). Cells were then washed and processed for electron microscopy (EM). Alternatively, cells were incubated at 4°C with 40 nM TeNT $H_C$ tagged with the vesicular stomatitis virus protein G epitope (VSVG) (Lalli et al., 1999) for 20 minutes, washed three times with 0.2% BSA in Hanks' buffer and blocked with 2% BSA, 0.25% porcine skin gelatin, 0.2% glycine, 15% fetal calf serum in PBS (blocking buffer) for 15 minutes at 4°C. Cells were then treated with mouse anti-VSVG antibody (1:80) (Lalli et al., 1999) diluted in PBS containing 1% BSA, 0.25% skin gelatin (antibody dilution buffer) for 30 minutes at 4°C. After rinsing in Hanks' buffer, cells were incubated with 10 nm gold-conjugated goat anti-mouse IgG (1:100; British BioCell International) for 25 minutes at 4°C, washed with Hanks' buffer and immediately fixed or warmed to 37°C for 5 or 20 minutes before fixation. MNs were post-fixed with 1% osmium tetroxide for 30 minutes, washed, dehydrated in ascending ethanol series and embedded in araldite over 2 days. Thin sections were stained with methanolic uranyl acetate and lead citrate for morphological examination or aqueous uranyl acetate for immunogold samples. Sections were then observed with a Jeol 1010 transmission electron microscope.

### Immunofluorescence

MNs were fixed with 4% paraformaldehyde, 20% sucrose in PBS for 15 minutes at room temperature, washed with PBS, incubated with 50 mM $NH_4Cl$ for 20 minutes, rinsed and permeabilized with blocking buffer containing 0.1% Triton X-100 for 15 minutes. Primary antibodies were applied in antibody dilution buffer for 1 hour. After rinsing with PBS, secondary antibodies were applied for 25 minutes. Cells were then washed and mounted with Mowiol 4-88 (Harco). For F-actin detection cells were incubated with Alexa Fluor 488 phalloidin (1:50) in PBS for 20 minutes after blocking. Imaging was performed with a Zeiss LSM 510 confocal microscope using a 63×, 1.40 NA Plan-Apochromat oil-immersion objective.

## Results

### Rat MNs bind and internalize fluorescent TeNT $H_C$ through a specific mechanism

To visualize retrograde transport in living MNs we designed a probe based on a recombinant nontoxic fragment of TeNT

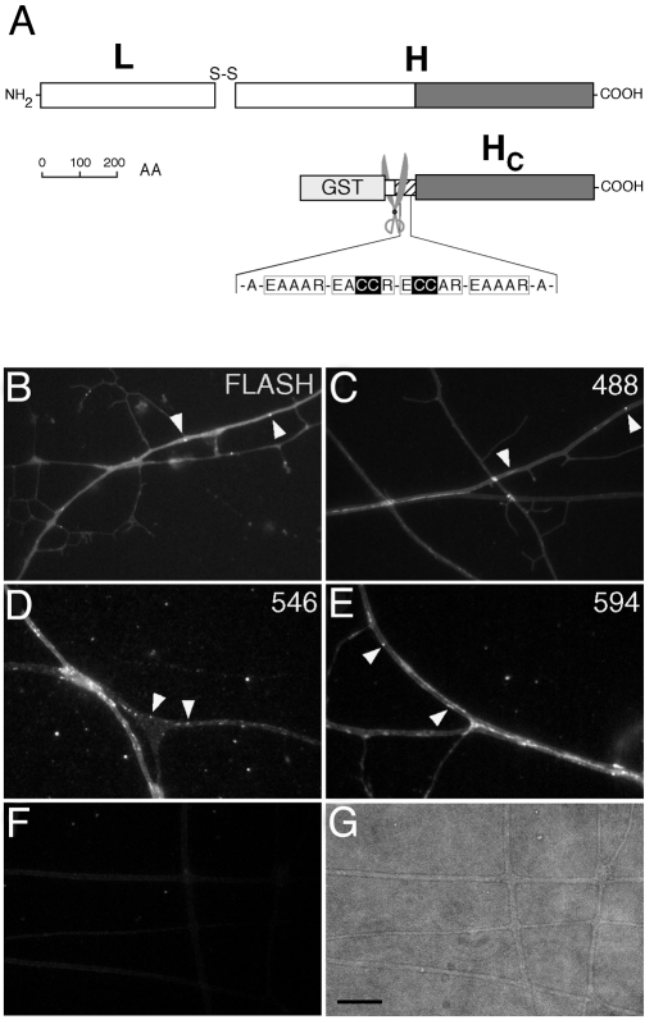


**Fig. 1.** TeNT $H_C$ labelled with different fluorophores is specifically transported in MNs. (A) TeNT and the recombinant TeNT $H_C$ used in this study. TeNT is composed of two chains (H and L). The $H_C$ fragment (dark grey) is responsible for neurospecific binding and retrograde transport. TeNT $H_C$ with a cysteine-rich tag at the N-terminus (hatched box) was expressed as a glutathione S-transferase (GST) fusion protein. The boxed segments are predicted to form α-helices with cysteines (in black) favourably oriented to bind FLASH or Alexa maleimides. Scissors indicate the thrombin cleavage site. (B-G) Binding and internalization of TeNT $H_C$ in living rat MNs imaged by low-light microscopy. TeNT $H_C$-FLASH (B), TeNT $H_C$-Alexa488 (C), TeNT $H_C$-Alexa 546 (D) and TeNT $H_C$-Alexa594 (E) (all 40 nM) are internalized and transported in vesicular carriers (arrowheads). (F) Binding and transport of TeNT $H_C$-Alexa488 are abolished by pre-incubation with a 100× molar excess of native TeNT. (G) Phase contrast picture of the corresponding image in F. Bar, 10 μm.

(Lalli et al., 1999) tagged at the N-terminus with a cysteine-rich domain designed to covalently bind the biarsenical fluorescein derivative FLASH (Fig. 1A) (Griffin et al., 1998). This cysteine-rich tag is also the site of modification by other thiol-specific fluorescent reagents, such as the Alexa 488, 546 or 594 maleimides. Multiple fluorophores can be coupled to TeNT $H_C$ upstream of its coding sequence, avoiding the risk of perturbing the C-terminal portion, which is required for neurospecific binding (Schiavo et al., 2000). Fluorescent TeNT $H_C$ bound to purified rat MNs and was internalized in vesicular structures irrespective of the fluorophore used for labelling (Fig. 1B-E; arrowheads). These carriers are of endosomal origin, given that they were labelled by Texas Red-dextran, a general endocytic marker (Nakata et al., 1998) (data not shown). Incubation of MNs with fluorescent TeNT $H_C$ at 4°C followed by washing and warming to 37°C led to the appearance of vesicular carriers, suggesting that fluorescent TeNT $H_C$ internalization is due to a specific uptake mechanism and not to fluid phase endocytosis. Moreover, binding and internalization were prevented by pre-incubating MNs with an excess of TeNT (Fig. 1F,G), showing that fluorescent TeNT $H_C$ interacts with the same surface receptors as the native holotoxin in living motor neurons.

To characterize TeNT $H_C$ carriers at an ultrastructural level, we analysed their morphology by EM using VSVG-tagged TeNT $H_C$ (Lalli et al., 1999) followed by anti-VSVG primary antibody and 10 nm gold-conjugated secondary antibody. At 4°C TeNT $H_C$ bound to the axonal plasma membrane of MNs (Fig. 2A) and accumulated at coated invaginations (Fig. 2B), synaptic sites and neurite contacts (Fig. 2C,D), as observed with fluorescent TeNT $H_C$ in living cells (data not shown). When neurons were subsequently shifted to 37°C for 5 minutes, gold particles were found in deep pits and coated vesicles (Fig. 2E,F). After 20 minutes at 37°C, TeNT $H_C$ was detected in uncoated tubulo-vesicular and round endocytic structures (Fig. 2G,H), consistent with the pleiomorphic retrograde carriers observed in living MNs by time-lapse fluorescence microscopy (Lalli and Schiavo, 2002). By EM, the diameter of the vesicular compartments varied between 50 and 100 nm, whereas the length of tubular structures was 2-3 μm. Similar results were obtained by using gold-conjugated TeNT $H_C$ and are consistent with a previous study performed with TeNT in mixed spinal cord cells (Parton et al., 1987).

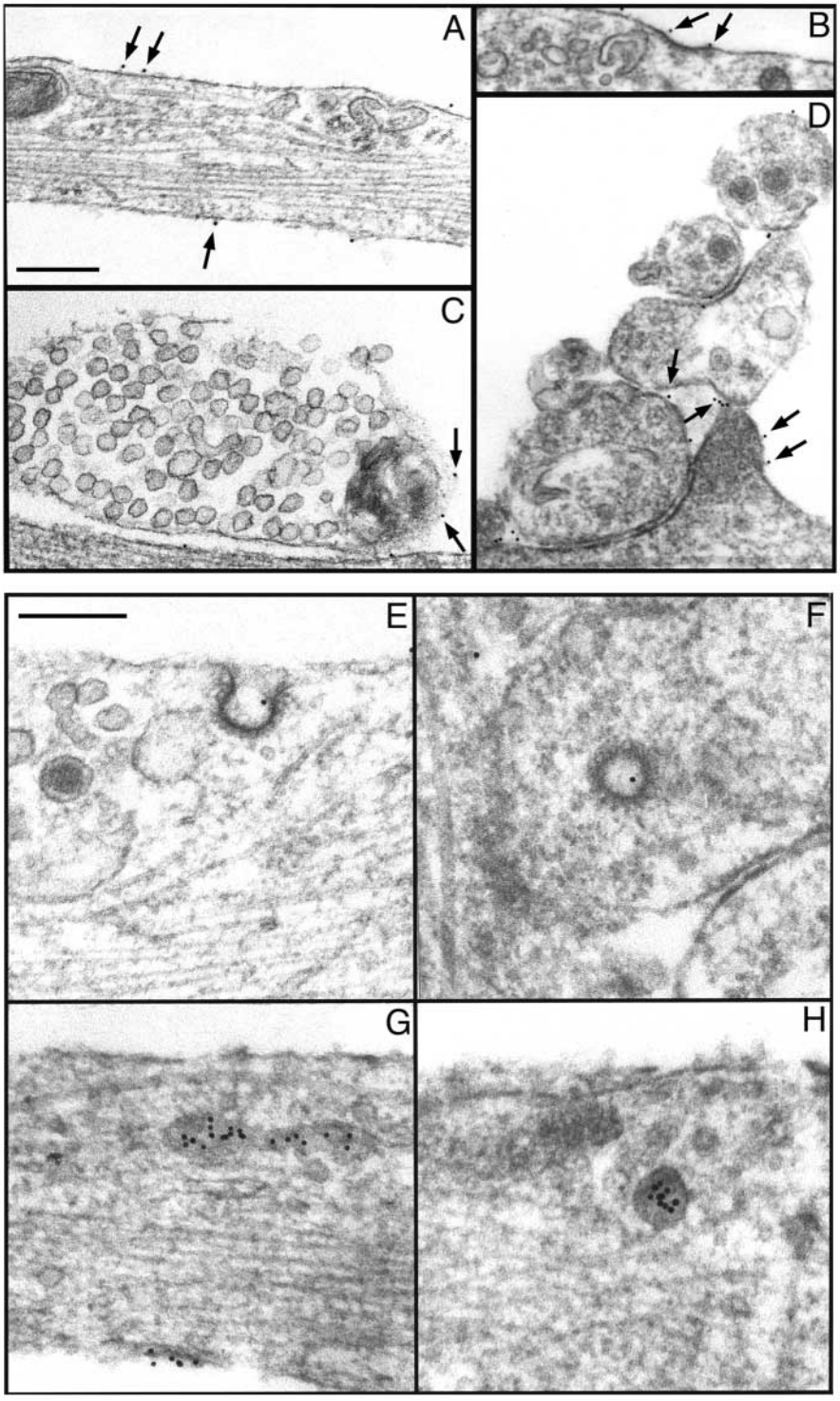


**Fig. 2.** Structures associated with TeNT $H_C$ binding and internalization. (A-D) Distribution of TeNT $H_C$ observed by EM in MNs after incubation with TeNT $H_C$ at 4°C followed by 10 nm gold-conjugated antibody. Gold (arrows) is found along neurite surfaces (a) and in forming coated pits (B). TeNT $H_C$ is also observed at synaptic sites (C) and neurite contacts (D). (E-H) MNs were treated as in A-D, washed and then warmed to 37°C for 5 (E and F) or 20 minutes (G and H). TeNT $H_C$ is found in coated pits (E) and coated vesicles (F), whereas at later internalization timepoints gold particles are observed in tubular (G) and round organelles (H). Control samples where TeNT $H_C$ was omitted showed negligible gold labelling. Bars, 0.2 μm.

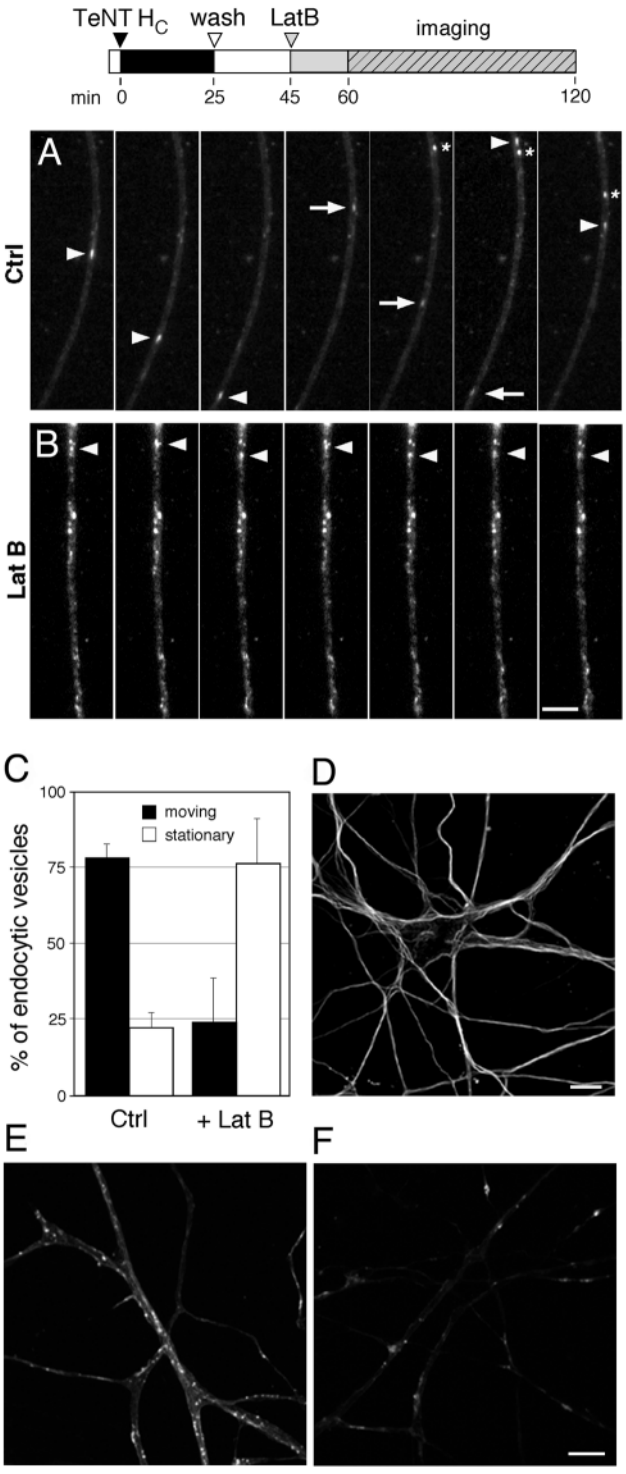


**Fig. 3.** Retrograde transport of TeNT $H_C$ depends on F-actin. A scheme of the experiment is shown at the top. MNs were treated with DMSO (Ctrl) (A) or with 0.5 μM Lat B (B). Intervals between frames are 5 seconds. Cell bodies are located at the bottom. (A) Control neurons display retrograde transport (arrowhead, arrow, asterisk). See video 1. (B) Lat B causes the majority of carriers to stop or oscillate (arrowhead). See video 2. (C) Quantitative analysis of TeNT $H_C$ transport after F-actin disruption. Carriers were classified as stationary/oscillatory when the extent of the movement did not lead to any significant progression (<0.2 μm). Results are expressed as a percentage of the total carriers observed (control = 437, Lat B = 315). Bars represent the s.d. of four independent experiments (P=0.01). (D) Treatment with Lat B does not affect MTs visualized by an anti-β-tubulin antibody. F-actin staining in MNs (E) disappears after Lat B treatment (F). Bars, 5 μm (A,B and E,F) and 10 μm (D).

### TeNT $H_C$ retrograde transport depends on both F-actin and microtubules

Fast axonal retrograde transport is dependent on MTs and MT-dependent motors (Hirokawa, 1998; Goldstein and Yang, 2000). However, other studies have shown the involvement of F-actin in organelle motility (Brady et al., 1984; Kuznetsov et al., 1992; Bearer et al., 1993; Morris and Hollenbeck, 1995; Tabb et al., 1998), leading to the hypothesis that the two cytoskeletal systems cooperate in vesicle transport (Langford, 1995; Goode et al., 2000). We therefore investigated the effect of F-actin or MT disruption on TeNT $H_C$ retrograde movement. Drugs were added to cells after TeNT $H_C$ internalization, when retrograde-moving compartments were already visible. Incubation of MNs with control medium (see Materials and Methods) did not affect the transport of TeNT $H_C$ carriers (Fig. 3A and video 1), whereas treatment with the F-actin-disrupting drug latrunculin B (Lat B) caused the majority of the vesicles to stop or oscillate (Fig. 3B and video 2). We quantified the inhibitory effect of Lat B by counting the moving and stationary/oscillating vesicles in untreated and drug-treated cells (Fig. 3C). In untreated MNs, 80.1±5.1% of the vesicles moved in retrograde fashion with speed ranging between 0.2 and 3.6 μm/second (Lalli and Schiavo, 2002), whereas 19.9±5.1% were stationary. Lat B treatment led to a significant increase in the number of resting organelles (76.0±15.0%). Moving carriers represented only 24.0±14.2% of the total vesicles observed and were characterized by a reduced average speed ranging from 0.1 to 0.7 μm/second. Similar results were obtained using another F-actin-disrupting agent, swinholide A (data not shown). In control MNs, F-actin stained by fluorescent phalloidin showed a homogeneous distribution along neurites with sparse bright puncta (Fig. 3E). This staining disappeared after Lat B treatment (Fig. 3F). In the timecourse of our analysis, Lat B did not alter neurite morphology nor MT distribution as revealed by immunofluorescence with an anti-β-tubulin antibody (Fig. 3D) and by quantitative EM analysis of neurite cross-sections (Fig. 4C). It is therefore very unlikely that in our experimental conditions the disruption of the actin cytoskeleton causes a generalized neurite collapse or re-organization of the cellular cytoskeleton, indirectly affecting other actin-independent processes. To further exclude potential problems linked to acute F-actin depolymerization, MNs were differentiated for 3 days in the presence of LatB or cytochalasin B, a protocol resembling the chronic treatment previously reported in the literature (Morris and Hollenbeck, 1995). In addition to minor morphological alterations and a reduction of TeNT $H_C$ internalization, long-term treatment with LatB caused an inhibition of retrograde transport with a significant increase of still/oscillating carriers, which is in agreement with the results shown in Fig. 3C. As previously reported (Morris and Hollenbeck, 1995), neurite morphology after chronic treatment with cytochalasin B was dramatically altered (data not shown),

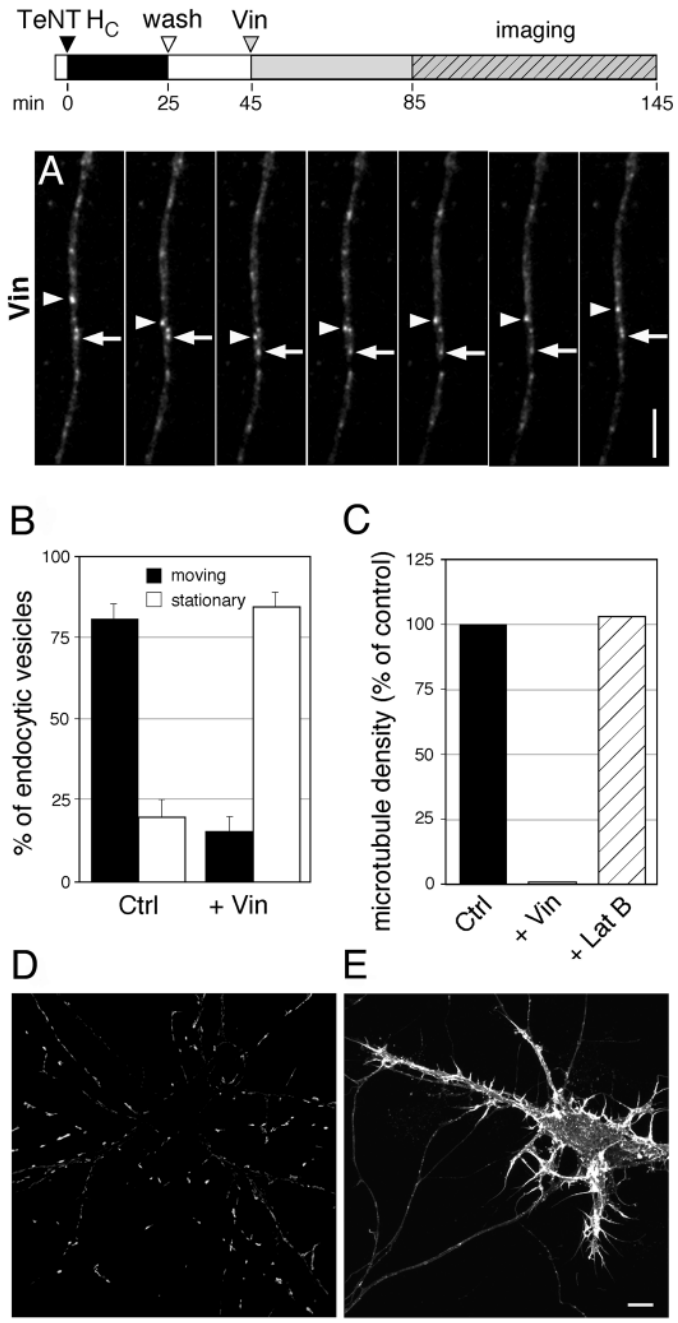


**Fig. 4.** Retrograde transport of TeNT $H_C$ depends on intact MTs. A scheme of the experiment is shown at the top. (A) MNs were incubated with TeNT $H_C$-Alexa488 and treated with 5 μM Vin after the appearance of fluorescent carriers. The majority of carriers stops or oscillates (arrowhead, arrow). Intervals between frames are 20 seconds. The cell body is located at the bottom. See video 3. (B) Quantitative analysis of TeNT $H_C$ transport after MT disruption. Results are expressed as a percentage of the total carriers observed (control = 364, Vin = 361; *n*=2). (C) EM analysis of neurite cross-sections shows that MTs are absent in Vin-treated cells, whereas their density is unchanged in Lat B-treated cells. Data are expressed as a percentage of MT density observed in untreated MNs (control = 58; Vin = 36; Lat B = 24 neurites). The same cells used in A were immunostained for β-tubulin. Treatment with Vin causes the accumulation of tubulin in paracrystals (D). Vin treatment is specific and does not affect F-actin visualized with fluorescent phalloidin (E). Bars, 5 μm (A) and 10 μm (D,E).

hampering any further analysis of retrograde transport under these conditions.

Vincristine (Vin) has been shown to specifically disrupt MTs in neurons (Allison et al., 2000). Acute treatment with this drug greatly reduced retrograde movement (Fig. 4A and video 3), as shown by a threefold increase of the number of stationary/oscillating vesicles compared with control cells (84.0±4.5%; Fig. 4B). Vin-treated cells showed a 99% decrease of MT density compared with untreated cells, on the basis of quantitative EM analysis of neurite cross-sections (Fig. 4C). In Vin-treated MNs, only tubulin paracrystals could be observed (Fig. 4D, compare with Fig. 3D), whereas F-actin distribution was similar to untreated controls (Fig. 4E). Although the short-term treatment with Vin is well tolerated, chronic treatment at low dosage is toxic for MNs, causing detachment and cell death (data not shown). Therefore, this condition has not been further used for quantitative analysis. Treatment of MNs with the MT-depolymerising agent nocodazole only reduced retrograde movement (data not shown). However, morphometric EM analysis of neurite cross-sections revealed the presence of nocodazole-resistant MTs (25% of control cells; data not shown), strongly suggesting that the partial inhibition seen with nocodazole is due to an incomplete depolymerization of MT rather than to MT-independent axonal transport. Taken together, these data show that retrograde transport of TeNT $H_C$ is dependent on the integrity of both MTs and actin cytoskeleton.

## Efficient TeNT $H_C$ retrograde transport relies on multiple MT-based motors

We then chose a pharmacological approach to characterize the motors required for TeNT $H_C$ retrograde transport. To selectively impair MT-based motors, we used the well-established dynein inhibitor EHNA (Penningroth et al., 1982; Reynolds et al., 1998) and the kinesin inhibitor aurintricarboxylic acid (AA) (Hopkins et al., 2000). AA has been recently identified via a structure-based computer screening for kinesin-binding molecules using human conventional kinesin as template (Hopkins et al., 2000). It has been shown to have a broad specificity for members of the kinesin superfamily (conventional kinesin, ncd C-terminal kinesin and Unc104/KIF1) (Vale, 2003) and an $IC_{50}$ in the low micromolar range (0.5-1.4 μM), which is comparable to that of the only other known kinesin inhibitor, adocia sulfate-2 (Sakowicz et al., 1998). At the concentration used in the assay (10 μM), AA inhibits kinesin specifically, as the F-actin-dependent activity of myosin II remains unchanged (Hopkins et al., 2000).

TeNT $H_C$-positive carriers from control and treated cells were tracked, and the distribution of speed values calculated between two consecutive frames was plotted. Control cells consistently showed a speed distribution profile centred at 0.8-1 μm/second, extending up to 3.6 μm/second in the retrograde direction (Fig. 5A-C, black bars). This distribution is consistent with the rates calculated for TeNT retrograde transport in vivo, ranging between 0.8 and 3.6 μm/second (Schiavo et al., 2000). Interestingly, dynein inhibition with EHNA led to a decrease of fast movements but did not completely stop TeNT $H_C$ retrograde transport (Fig. 5A, white bars). Incubation with the kinesin inhibitor AA had a less pronounced effect on transport

than dynein impairment. However, AA still caused a decrease of high speed values accompanied by a parallel increase of pauses and anterograde movements, represented conventionally by negative speed values (Fig. 5B, white bars). To ascertain whether different MT-based motors act synergistically in promoting efficient TeNT $H_C$ retrograde transport, we simultaneously incubated MNs with EHNA and AA. However, these drugs had an effect on the speed distribution similar to that observed with EHNA alone (Fig. 5C, white bars; compare with Fig. 5A).

The speed distributions of TeNT $H_C$ alone or after treatment with motor inhibitors were further analysed by applying a multiple Gaussian curve fit. For all experiments ($n$=7), the speed profile of TeNT $H_C$ carriers is best described by the sum of three distinct components identified by Gaussian distributions centred at 0±0.11, 0.53±0.31 and 1.15±0.70 μm/second (Fig. 5D) ($R^2$=0.997). This trimodal representation allowed us to determine the relative contribution of each speed component to retrograde transport, with the fastest component (1.15 μm/second) responsible for more than 70% of the total movements (Fig. 5E, black bars and Table 1).

In EHNA-treated MNs, we observed a dramatic decrease of the fast (1.15 μm/second) speed component, whereas the intermediate (0.53 μm/second) was unaffected (Fig. 5E, white bars and Table 1). EHNA also caused an increase in the frequency of pauses and of slow, short anterograde movements (Fig. 5A), resulting in oscillation of TeNT $H_C$ carriers. In agreement with this observation, the incidence of reversal (number of changes of direction per organelle) in EHNA-treated cells increased more than tenfold compared with untreated samples (10.3±2.4; 122 and 281 tracked carriers in drug-treated and control cells, respectively; $n$=3 independent experiments). This result confirms and extends our recent report that the fast component of axonal retrograde transport is impaired in mice carrying mutations in dynein heavy chain (Hafezparast et al., 2003).

AA treatment also caused a decrease of the fast component, although less marked than the one observed with EHNA, whereas the contribution of the intermediate speed component remained similar to the control (Fig. 5E, hatched bars and Table 1). Simultaneous incubation with EHNA and AA led to an inhibition of the fast component similar to the one observed with EHNA alone. By contrast, the intermediate component remained unaffected (Fig. 5E, grey bars). This residual movement observed after inhibition of dynein and kinesins might be due to the involvement of actin-based motors, as

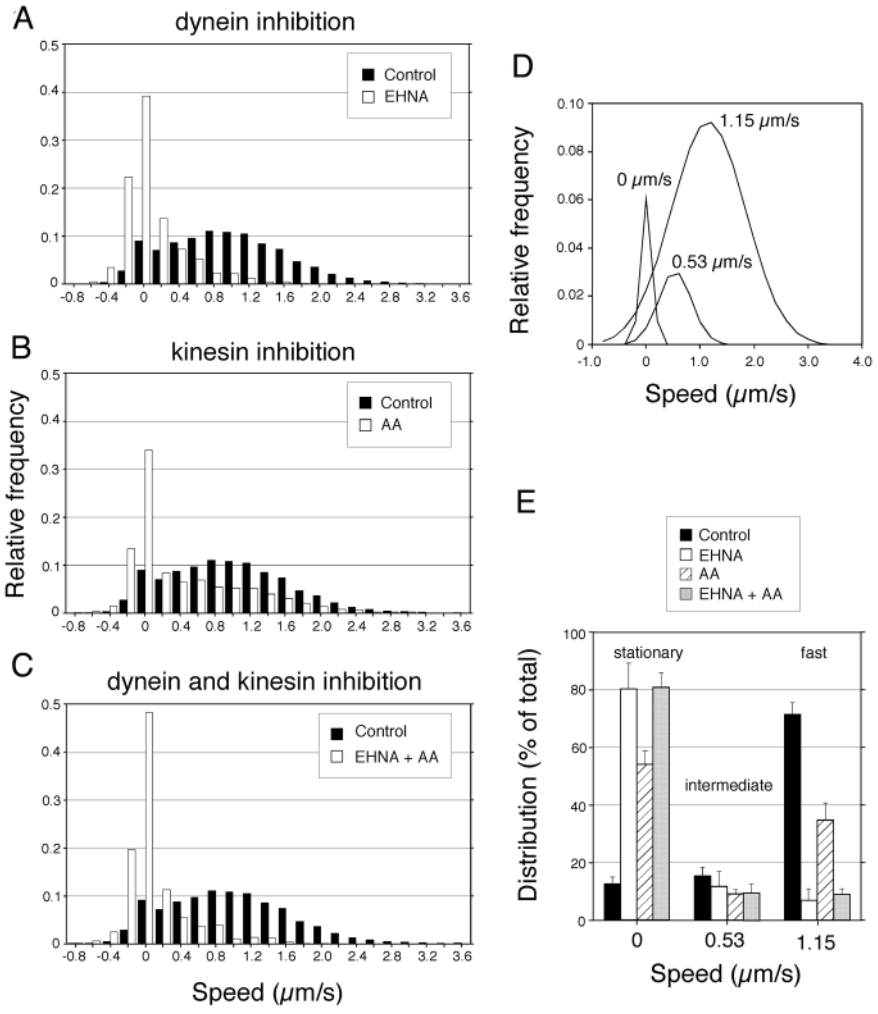


**Fig. 5.** Efficient retrograde transport of TeNT $H_C$ depends on multiple MT-based motors. (A-C) Distribution of speed values observed between two consecutive frames for TeNT $H_C$-Alexa488 carriers (interval = 5 seconds). Retrograde movement is conventionally shown as positive. (A) Effect of dynein inhibition on TeNT $H_C$ transport. MNs were incubated with control medium (718 carriers, $n$=7 independent experiments; black bars) or with 1 mM EHNA (142 carriers; $n$=4; white bars). Note the drastic decrease in the frequency of fast retrograde speed movements and the increase in pauses and slow anterograde movements. (B) Effect of kinesin inhibition on TeNT $H_C$ transport. Incubation of MNs with 10 μM AA (308 carriers; $n$=3; white bars) increases the frequency of pauses and of slow anterograde movements, and induces a decrease of high speed values which is less marked than after EHNA treatment. (C) Simultaneous treatment of MNs with EHNA and AA (57 carriers; $n$=2; white bars) has similar effects on TeNT $H_C$ transport to EHNA alone. (D) The speed distribution profile of TeNT $H_C$ carriers in rat MNs is best described by the sum of three Gaussian components, centred at 0, 0.53 and 1.15 μm/second (718 carriers; $n$=7). Quantification of these speed components in the presence and absence of motor inhibitors allowed us to analyse the contribution of different molecular motors to retrograde transport (E). EHNA (white bars) abolished the fast component and caused a correspondent increase of pauses, whereas the intermediate component remained unaltered compared with control cells (black bars). AA alone (hatched bars) increased the frequency of stationary periods while reducing the contribution of the fast component. Simultaneous treatment of cells with EHNA and AA (grey bars) led to the same effects observed with EHNA alone. Error bars represent mean values ± s.e.m.

**Table 1. Quantification of the effects of inhibitors of MT-based molecular motors on the speed of TeNT $H_C$ carriers**

| | Control (*n*=7) | EHNA (*n*=4) | AA (*n*=3) | EHNA +AA (*n*=2) |
|---|---|---|---|---|
| Stationary (0 μm/second) | 12.8±2.5 | 80.8±8.7 | 54.1±4.8 | 81.3±6.9 |
| Intermediate (0.53 μm/second) | 15.4±3.0 | 11.7±5.2 | 10.0±1.3 | 9.39±4.2 |
| Fast (1.15 μm/second) | 71.7±4.1 | 7.43±3.8 | 35.9±5.6 | 9.31±2.7 |
| $R^2$ | 0.997 | 0.971 | 0.977 | 0.979 |

Contributions of the three kinetic components to the speed distribution of TeNT $H_C$ carriers in control MNs and in MNs treated with the indicated MT-based motor inhibitors. The contributions of the single speed components were determined as described in Materials and Methods and expressed as a percentage of the total (mean±s.e.m.). The number of independent experiments included in the analysis is indicated (*n*), together with the correlation coefficient ($R^2$) for the fitted trimodal Gaussian distribution.

predicted by the requirement for F-actin in TeNT $H_C$ transport observed in Fig. 3. To test this hypothesis, we used the drug 2,3 butanedione monoxime (BDM, 10 mM) as a broad-spectrum myosin inhibitor (Cramer and Mitchison, 1995; Lin et al., 1996; Prekeris and Terrian, 1997; Duran et al., 2003). Simultaneous treatment of MNs with EHNA, AA and BDM completely stopped TeNT $H_C$ carriers (data not shown). This result supports the idea that myosins play a role in retrograde transport and indicates that the residual movement observed after simultaneous treatment with EHNA and AA was not due to an incomplete inhibition of MT-dependent motors.

This evidence points to the presence on TeNT $H_C$ carriers of multiple types of motors contributing to fast axonal retrograde transport. Moreover, it suggests that TeNT $H_C$ transport relies mainly on dynein, but requires kinesins and possibly actin-based motors to achieve optimal efficiency.

### Myosin Va is required for efficient retrograde transport in mammalian MNs

To identify myosins involved in retrograde movement of TeNT $H_C$ carriers, we performed an immunofluorescence screening in spinal cord MNs for different types of myosins previously reported to have a role in vesicular transport in neurons (DePina and Langford, 1999; Bridgman and Elkin, 2000; Wu et al., 2000; DeGiorgis et al., 2002; Brown, 2003). We detected colocalization of TeNT $H_C$ carriers only with myosin Va, a motor protein participating in the transport of several types of organelles in vitro and in vivo (Wu et al., 2000; Langford, 2002) (Fig. 6A-C, arrowheads).

To clarify whether myosin Va is functionally important for axonal retrograde transport, we tested MNs from wild-type and homozygous *dilute lethal* (myosin Va null) mice (Mercer et al., 1991) for their ability to transport TeNT $H_C$. Retrograde movement of fluorescent TeNT $H_C$ in *dilute lethal* MNs was clearly impaired compared with wild-type cells (Fig. 6D,E, arrowheads, asterisks; see also video 4). Wild-type MNs displayed a speed distribution curve centred at 0.8 μm/second and reaching a maximum value of 3 μm/second (Fig. 6F, filled circles). Kinetic analysis of TeNT $H_C$ carriers in MNs from *dilute lethal* animals revealed both a decrease in the frequency of high-speed values and an increase of pauses and slow bidirectional movements (Fig. 6F, empty circles). This led to a substantial rise of oscillations, as further indicated by the ~eightfold increase of the incidence of reversal of TeNT $H_C$ carriers in *dilute lethal* compared with wild-type MNs (7.78±2.3; 141 and 357 carriers in *dilute lethal* and wild-type cells, respectively; *n*=3). The speed distribution curve for TeNT $H_C$ transport in wild-type mice MNs can be best described by the sum of three distinct Gaussian profiles centred at 0, 0.53 and 0.95 μm/second, respectively (Fig. 6G). As observed in rat MNs, the intermediate (0.53 μm/second) and fast (0.95 μm/second) components account for more than 80% of the carriers. TeNT $H_C$ transport in *dilute lethal* MNs showed a severe reduction of the fastest (0.95 μm/second) speed component, with a corresponding increase in the frequency of pauses, whereas the intermediate speed carriers remain unaltered (Fig. 6G, white bars). These data reveal a novel role of myosin Va in axonal retrograde transport and suggest that this myosin is required for fast retrograde movement in mammalian MNs.

## Discussion

In this study, we have used a fluorescent fragment of TeNT, which is specifically recruited to a fast axonal retrograde transport pathway (Lalli and Schiavo, 2002), as a probe to analyse the cytoskeletal and motor requirements for this process in mammalian MNs. The retrograde transport of TeNT $H_C$ is both MT- and F-actin-dependent. Fast axonal transport is known to rely on an intact MT cytoskeleton (Goldstein and Yang, 2000). However, we found a dramatic effect of F-actin depolymerization on retrograde transport, under conditions preserving the integrity of MTs. After F-actin disruption by Lat B and other F-actin-depolymerising agents, the great majority of TeNT $H_C$ carriers were stationary or oscillated. This result indicates that actin microfilaments are required for the directional transport of axonal organelles, as previously suggested by experiments on isolated squid axoplasm (Brady et al., 1984). EM studies have revealed a tight association of MTs with actin microfilaments (Fath and Lasek, 1988; Bearer and Reese, 1999) that could be important not only for maintaining the structural integrity of the axon, but also for supporting fast transport. In sympathetic neurons, disruption of F-actin led to a significant increase in the speed of bidirectionally moving mitochondria or myosin V-associated organelles (Morris and Hollenbeck, 1995; Bridgman, 1999), suggesting that actin-based motility is not strictly necessary for rapid axonal movement. However, in MNs, fast retrograde transport requires the simultaneous presence of MTs and F-actin. Different neuronal systems might therefore use motors with distinct cytoskeletal requirements, depending on the type of organelle transported, its direction and the differentiation state of the neurons.

An important implication of our findings is that both MT- and actin-based motors power the movement of TeNT $H_C$ carriers in MNs. Dynein is probably the major motor responsible for TeNT $H_C$ retrograde transport, as its inhibition caused the largest decrease in the speed of TeNT $H_C$ carriers and an increase in the frequency of stationary pauses and incidence of reversal. The central role for dynein in axonal transport is underscored by the finding that point mutations in dynein heavy chain specifically impair fast retrograde transport in mice, generating pathological conditions closely resembling amyotrophic lateral sclerosis (Hafezparast et al., 2003).

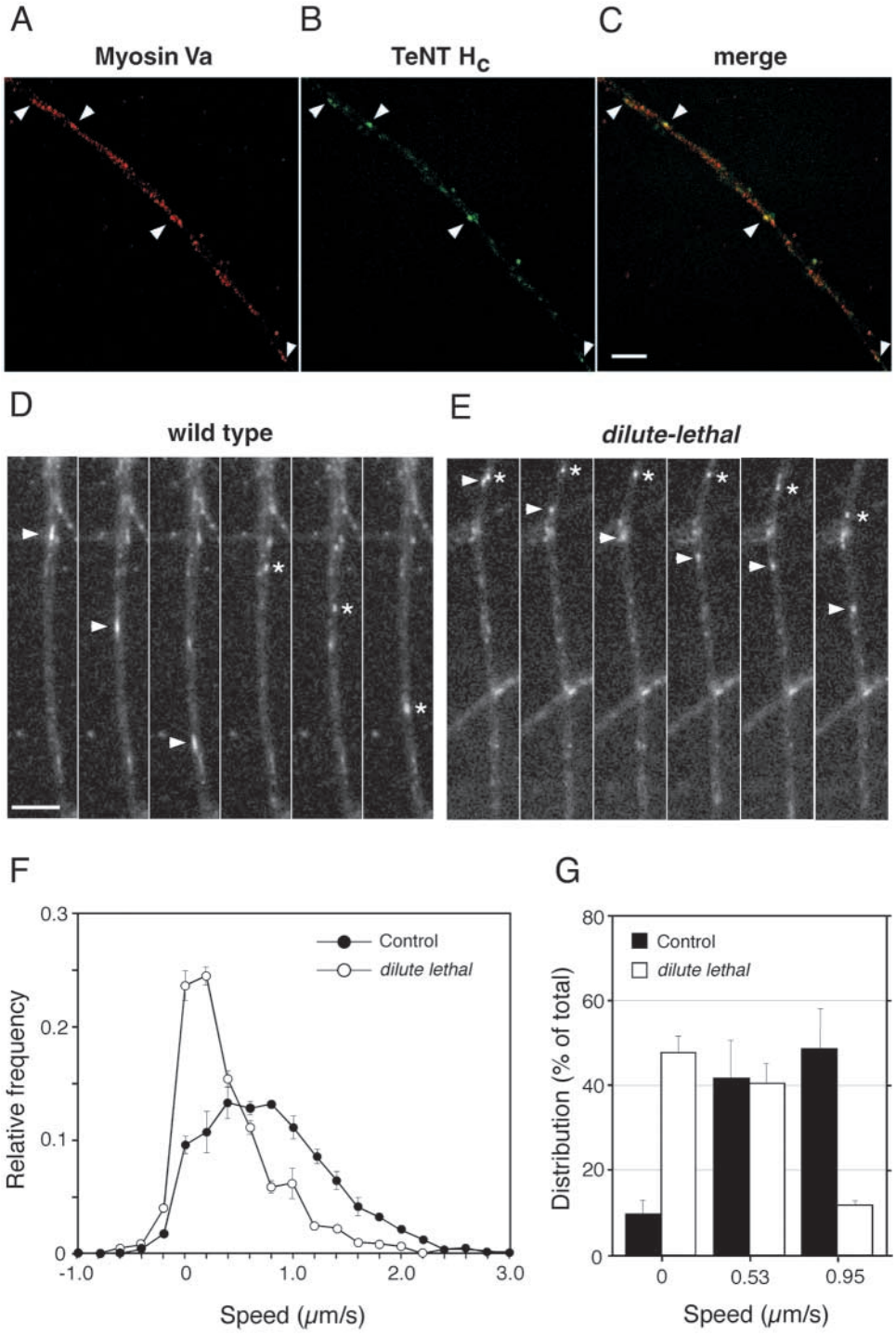


**Fig. 6.** Myosin Va is required for efficient retrograde transport in living MNs. (A) In rat MNs myosin Va shows an abundant punctate distribution and co-localises with TeNT $H_C$-Alexa 488 carriers (B, arrowheads). (C) Merged image of A and B. (D,E) Time-lapse imaging of TeNT $H_C$-Alexa 488 retrograde carriers (arrowheads, asterisks) in an axon of a wild-type (D) or a *dilute lethal* (E) mouse MN. Intervals between frames are 5 seconds. The cell body is located at the bottom in both D and E. Bars, 5 μm. See video 4. (F) Relative frequencies of speed values measured between two consecutive frames (interval = 5 seconds) for TeNT $H_C$ carriers in wild-type MNs (193 carriers, filled circles; three embryos) and *dilute lethal* MNs (91 carriers, empty circles; two embryos). Wild-type and *dilute lethal* embryos are derived from the same litter. Retrograde movement is conventionally shown as positive. (G) In mouse MNs, the speed distribution profile of TeNT $H_C$ is best described by the sum of three Gaussian curves centred at 0, 0.53 and 0.95 μm/second. A decrease of the fast component and an increase of pauses are observed in *dilute lethal* MNs (white bars), whereas the intermediate component remains unaltered relative to wild-type cells (black bars). Data are derived from the analysis of 357 carriers from five wild-type embryos and 141 carriers from three *dilute lethal* embryos. Error bars indicate mean ± s.e.m.

Moreover, a missense mutation in the dynein-interacting protein dynactin/p150$^{glued}$ causes lower motor neuron disease in humans (Puls et al., 2003), confirming the functional link between fast axonal retrograde transport, cytoplasmic dynein and neuronal degeneration.

Regardless of the central role played by dynein in fast retrograde transport, several results indicate that multiple motors are involved in this process. First, blocking dynein activity by a pharmacological approach or via specific mutations in its core subunit (Hafezparast et al., 2003) did not lead to a complete halt of TeNT $H_C$ carriers. Second, the speed distribution curve of TeNT $H_C$ endosomes shows multiple peaks. Third, a kinesin inhibitor also affected transport, although less dramatically. Moreover, cytoplasmic dynein supports long-range intracellular movements of cargo in vivo but does not appear to be a processive motor (Hirakawa et al., 2000; King and Schroer, 2000). It could therefore require other MT and actin-based motors to achieve maximal speed and processivity. Inhibition of kinesins slowed the movement of TeNT $H_C$ carriers in the presence of active dynein but did not

produce any synergistic inhibitory effect when dynein was blocked by EHNA. The dynein complex could therefore act not only as a main retrograde motor, but also as a regulator of the activity of other motors associated with TeNT $H_C$ carriers. Studies in yeast and *Drosophila* point to a functional interaction of dynactin/p150$^{glued}$ with kinesins during mitosis and in fast axonal transport (Blangy et al., 1997; Martin et al., 1999) and have shown its involvement in the coordination of plus- and minus-end-directed motors (Gross et al., 2002b). In the case of mammalian MNs, it is tempting to speculate that the dynein/dynactin complex regulates the engagement of multiple retrograde motors, allowing the cargo to move more efficiently along the axon.

The residual movement observed after the inhibition of MT-based motors suggests that other molecules, such as one or more myosins, are also implicated in retrograde transport. By using our retrograde transport assay in *dilute lethal* mice we have shown that myosin Va is required for this process. Studies on the dynamics of organelles associated with myosin Va (Wu et al., 1998; Bridgman, 1999; Al-Haddad et al., 2001), together with the demonstration that myosin V is a processive motor (Mehta et al., 1999), support the hypothesis that this protein plays an important role in organelle transport. In sympathetic neurons, the movement of myosin Va-associated organelles is bidirectional. However, these organelles become anterogradely biased in *dilute lethal* neurons, implying the participation of myosin Va in retrograde transport (Bridgman, 1999). Recently, myosin Va has been shown to control neurofilament density, its ablation determining an increase in neurofilament number in vivo (Rao et al., 2002). This raises the possibility that *dilute lethal* neurons show a general impairment of axonal transport. However, the observed increase of the maximum speed of axonal vesicles in these neurons (Bridgman, 1999), together with their biased directionality, strongly argues against this scenario.

On the basis of this previous work (Bridgman, 1999), myosin Va has been proposed to dampen organelle movement, as seen in mouse melanosomes and phagosomes (Wu et al., 1998; Al-Haddad et al., 2001). This and other experimental findings have been recently summarized by the 'cooperative/capture mechanism' (Wu et al., 1998). According to this model, myosin Va anchors melanosomes on the peripheral random network of actin microfilaments, preventing them from moving centripetally on MTs to reach the perinuclear region. In an extension of this model, Al-Haddad and colleagues proposed an 'antagonistic/cooperative mechanism', whereby actin-dependent digressions powered by myosin Va antagonize dynein-dependent phagosome motility (Al-Haddad et al., 2001). A prediction of this model is that the absence of myosin Va in *dilute lethal* MNs should result in a faster retrograde transport compared with wild-type neurons. However, our findings argue against an inhibitory role of myosin Va, as fast retrograde axonal transport is impaired in myosin Va null MNs.

These apparent differences in myosin Va function can be reconciled by assuming that its contribution to organelle transport varies accordingly to the orientation of the actin cytoskeleton in each cell type. Myosin Va, a barbed-end-directed motor (Cheney et al., 1993), could contribute to fast retrograde transport in MNs by moving on actin filaments running co-axially with MTs and oriented with the barbed ends towards the cell body. Interestingly, mitochondria, which move bidirectionally, show a net retrograde transport in the absence of MTs in sympathetic neurons, implying the existence of F-actin with biased polarity in axons (Morris and Hollenbeck, 1995). Alternatively, these differences in myosin Va function could be attributed to a selective organelle-specific regulation, as shown for the myosin Va-dependent transport of endoplasmic reticulum in mitotic *Xenopus* egg extracts (Wöllert et al., 2002), the class V myosin Myo2p-driven movement of vacuoles (Ishikawa et al., 2003; Tang et al., 2003) and Myo4p-directed RNA transport (Kruse et al., 2002).

Our experimental data imply that myosin Va activity is coordinated with MT-based retrograde motors to ensure fast retrograde transport in mammalian MNs. In this system, myosin Va could power movement on F-actin, which serves as complementary tracks during MT-based transport. This might help carriers to dodge obstacles, similarly to what has been observed in *Xenopus* melanophores (Rogers and Gelfand, 2000; Gross et al., 2002a). In addition, myosin Va could contribute to fast transport by allowing movement on F-actin during transition from one MT to another, thus decreasing the probability of diffusional movements of organelles. Precise coordination between MT-based motors and myosin Va could be achieved through additional regulating factors or direct interaction. Both myosin Va and the intermediate chain of cytoplasmic dynein share an 8 kDa light chain (Mermall et al., 1998) able to dimerize (Benashski et al., 1997), suggesting that these two motors interact on the surface of a transport carrier. Deletion of myosin Va from a dynein-associated particle might impair the activity of the entire motor complex, providing the molecular explanation for the absolute requirement of both myosin Va and dynein for fast retrograde transport in this system. Discovering the molecular mechanisms responsible for the coordination between myosin Va and MT-based retrograde motors and the relationship between MTs and actin cytoskeleton in axons are challenging objectives for future studies.

We thank Drs P. C. Bridgman for the gift of anti-myosin Va antiserum, M. Seabra and R. Anders for the gift and handling of *dilute lethal* mice and J. Monypenny for help with video editing. We are grateful to Drs D. Ish-Horowicz, C. Reis e Sousa, S. Tooze and M. Way for critical reading of the manuscript. This work was supported by Cancer Research UK.

## References

**Al-Haddad, A., Shonn, M. A., Redlich, B., Blocker, A., Burkhardt, J. K., Yu, H., Hammer, J. A., III, Weiss, D. G., Steffen, W., Griffiths, G. et al.** (2001). Myosin Va bound to phagosomes binds to F-actin and delays microtubule-dependent motility. *Mol. Biol. Cell* **12**, 2742-2755.

**Allison, D. W., Chervin, A. S., Gelfand, V. I. and Craig, A. M.** (2000). Postsynaptic scaffolds of excitatory and inhibitory synapses in hippocampal neurons: maintenance of core components independent of actin filaments and microtubules. *J. Neurosci.* **20**, 4545-4554.

**Arce, V., Garces, A., de Bovis, B., Filippi, P., Henderson, C. E., Pettmann, B. and deLapeyriere, O.** (1999). Cardiotrophin-1 requires LIFRβ to promote survival of mouse motoneurons purified by a novel technique. *J. Neurosci. Res.* **55**, 119-126.

**Bearer, E. L. and Reese, T. S.** (1999). Association of actin filaments with axonal microtubule tracts. *J. Neurocytol.* **28**, 85-98.

**Bearer, E. L., DeGiorgis, J. A., Bodner, R. A., Kao, A. W. and Reese, T. S.** (1993). Evidence for myosin motors on organelles in squid axoplasm. *Proc. Natl. Acad. Sci. USA* **90**, 11252-11256.

**Benashski, S. E., Harrison, A., Patel-King, R. S. and King, S. M.** (1997).

Dimerization of the highly conserved light chain shared by dynein and myosin V. *J. Biol. Chem.* **272**, 20929-20935.

**Blangy, A., Arnaud, L. and Nigg, E. A.** (1997). Phosphorylation by p34cdc2 protein kinase regulates binding of the kinesin-related motor HsEg5 to the dynactin subunit p150. *J. Biol. Chem.* **272**, 19418-19424.

**Brady, S. T., Lasek, R. J., Allen, R. D., Yin, H. L. and Stossel, T. P.** (1984). Gelsolin inhibition of fast axonal transport indicates a requirement for actin microfilaments. *Nature* **310**, 56-58.

**Bridgman, P. C.** (1999). Myosin Va movements in normal and dilute-lethal axons provide support for a dual filament motor complex. *J. Cell Biol.* **146**, 1045-1060.

**Bridgman, P. C. and Elkin, L. L.** (2000). Axonal myosins. *J. Neurocytol.* **29**, 831-841.

**Brown, A.** (2003). Axonal transport of membranous and nonmembranous cargoes: a unified perspective. *J. Cell Biol.* **160**, 817-821.

**Brown, S. S.** (1999). Cooperation between microtubule- and actin-based motor proteins. *Annu. Rev. Cell Dev. Biol.* **15**, 63-80.

**Butowt, R. and von Bartheld, C. S.** (2003). Connecting the dots: trafficking of neurotrophins, lectins and diverse pathogens by binding to the neurotrophin receptor $p75^{NTR}$. *Eur. J. Neurosci.* **17**, 673-680.

**Cheney, R. E., O'Shea, M. K., Heuser, J. E., Coelho, M. V., Wolenski, J. S., Espreafico, E. M., Forscher, P., Larson, R. E. and Mooseker, M. S.** (1993). Brain myosin-V is a two-headed unconventional myosin with motor activity. *Cell* **75**, 13-23.

**Cramer, L. P. and Mitchison, T. J.** (1995). Myosin is involved in postmitotic cell spreading. *J. Cell Biol.* **131**, 179-189.

**DeGiorgis, J. A., Reese, T. S. and Bearer, E. L.** (2002). Association of a nonmuscle myosin II with axoplasmic organelles. *Mol. Biol. Cell* **13**, 1046-1057.

**DePina, A. S. and Langford, G. M.** (1999). Vesicle transport: the role of actin filaments and myosin motors. *Microsc. Res. Tech.* **47**, 93-106.

**Duran, J. M., Valderrama, F., Castel, S., Magdalena, J., Tomas, M., Hosoya, H., Renau-Piqueras, J., Malhotra, V. and Egea, G.** (2003). Myosin motors and not actin comets are mediators of the actin-based golgi-to-endoplasmic reticulum protein transport. *Mol. Biol. Cell* **14**, 445-459.

**Evans, L. L., Hammer, J. and Bridgman, P. C.** (1997). Subcellular localization of myosin V in nerve growth cones and outgrowth from dilute-lethal neurons. *J. Cell Sci.* **110**, 439-449.

**Evans, L. L., Lee, A. J., Bridgman, P. C. and Mooseker, M. S.** (1998). Vesicle-associated brain myosin-V can be activated to catalyze actin-based transport. *J. Cell Sci.* **111**, 2055-2066.

**Fath, K. R. and Lasek, R. J.** (1988). Two classes of actin microfilaments are associated with the inner cytoskeleton of axons. *J. Cell Biol.* **107**, 613-621.

**Ginty, D. D. and Segal, R. A.** (2002). Retrograde neurotrophin signaling: Trk-ing along the axon. *Curr. Opin. Neurobiol.* **12**, 268-274.

**Goldstein, L. S. and Yang, Z.** (2000). Microtubule-based transport systems in neurons: the roles of kinesins and dyneins. *Annu. Rev. Neurosci.* **23**, 39-71.

**Goode, B. L., Drubin, D. G. and Barnes, G.** (2000). Functional cooperation between the microtubule and actin cytoskeletons. *Curr. Opin. Cell Biol.* **12**, 63-71.

**Griffin, B. A., Adams, S. R. and Tsien, R. Y.** (1998). Specific covalent labeling of recombinant protein molecules inside live cells. *Science* **281**, 269-272.

**Gross, S. P., Tuma, M. C., Deacon, S. W., Serpinskaya, A. S., Reilein, A. R. and Gelfand, V. I.** (2002a). Interactions and regulation of molecular motors in *Xenopus* melanophores. *J. Cell Biol.* **156**, 855-865.

**Gross, S. P., Welte, M. A., Block, S. M. and Wieschaus, E. F.** (2002b). Coordination of opposite-polarity microtubule motors. *J. Cell Biol.* **156**, 715-724.

**Hafezparast, M., Klocke, R., Ruhrberg, C., Marquardt, A., Ahmad-Annuar, A., Bowen, S., Lalli, G., Witherden, A. S., Hummerich, H., Nicholson, S. et al.** (2003). Mutations in dynein link motor neuron degeneration to defects in retrograde transport. *Science* **300**, 808-812.

**Henderson, C. E., Bloch-Gallego, E. and Camu, W.** (1995). Purified embryonic motoneurons. In *Neural Cell Culture* (eds J. Cohen and G. P. Wilkin), pp. 69-81. Oxford: IRL Press.

**Herreros, J., Ng, T. and Schiavo, G.** (2001). Lipid rafts act as specialised domains for tetanus toxin binding and internalisation into neurons. *Mol. Biol. Cell* **12**, 2947-2960.

**Hirakawa, E., Higuchi, H. and Toyoshima, Y. Y.** (2000). Processive movement of single 22S dynein molecules occurs only at low ATP concentrations. *Proc. Natl. Acad. Sci. USA* **97**, 2533-2537.

**Hirokawa, N.** (1998). Kinesin and dynein superfamily proteins and the mechanism of organelle transport. *Science* **279**, 519-526.

**Hopkins, S. C., Vale, R. D. and Kuntz, I. D.** (2000). Inhibitors of kinesin activity from structure-based computer screening. *Biochemistry* **39**, 2805-2814.

**Huang, J. D., Brady, S. T., Richards, B. W., Stenolen, D., Resau, J. H., Copeland, N. G. and Jenkins, N. A.** (1999). Direct interaction of microtubule- and actin-based transport motors. *Nature* **397**, 267-270.

**Ishikawa, K., Catlett, N. L., Novak, J. L., Tang, F., Nau, J. J. and Weisman, L. S.** (2003). Identification of an organelle-specific myosin V receptor. *J. Cell Biol.* **160**, 887-897.

**King, S. J. and Schroer, T. A.** (2000). Dynactin increases the processivity of the cytoplasmic dynein motor. *Nat. Cell Biol.* **2**, 20-24.

**Kruse, C., Jaedicke, A., Beaudouin, J., Bohl, F., Ferring, D., Guttler, T., Ellenberg, J. and Jansen, R. P.** (2002). Ribonucleoprotein-dependent localization of the yeast class V myosin Myo4p. *J. Cell Biol.* **159**, 971-982.

**Kuznetsov, S. A., Langford, G. M. and Weiss, D. G.** (1992). Actin-dependent organelle movement in squid axoplasm. *Nature* **356**, 722-725.

**Lalli, G. and Schiavo, G.** (2002). Analysis of retrograde transport in motor neurons reveals common endocytic carriers for tetanus toxin and neurotrophin receptor $p75^{NTR}$. *J. Cell Biol.* **156**, 233-240.

**Lalli, G., Herreros, J., Osborne, S. L., Montecucco, C., Rossetto, O. and Schiavo, G.** (1999). Functional characterisation of tetanus and botulinum neurotoxins binding domains. *J. Cell Sci.* **112**, 2715-2724.

**Langford, G. M.** (1995). Actin- and microtubule-dependent organelle motors: interrelationships between the two motility systems. *Curr. Opin. Cell Biol.* **7**, 82-88.

**Langford, G. M.** (2002). Myosin V, a versatile motor for short-range vesicle transport. *Traffic* **3**, 859-865.

**Lin, C. H., Espreafico, E. M., Mooseker, M. S. and Forscher, P.** (1996). Myosin drives retrograde F-actin flow in neuronal growth cones. *Neuron* **16**, 769-782.

**Martin, M., Iyadurai, S. J., Gassman, A., Gindhart, J. G., Jr, Hays, T. S. and Saxton, W. M.** (1999). Cytoplasmic dynein, the dynactin complex, and kinesin are interdependent and essential for fast axonal transport. *Mol. Biol. Cell* **10**, 3717-3728.

**Mehta, A. D., Rock, R. S., Rief, M., Spudich, J. A., Mooseker, M. S. and Cheney, R. E.** (1999). Myosin-V is a processive actin-based motor. *Nature* **400**, 590-593.

**Mercer, J. A., Seperack, P. K., Strobel, M. C., Copeland, N. G. and Jenkins, N. A.** (1991). Novel myosin heavy chain encoded by murine dilute coat colour locus. *Nature* **349**, 709-713.

**Mermall, V., Post, P. L. and Mooseker, M. S.** (1998). Unconventional myosins in cell movement, membrane traffic, and signal transduction. *Science* **279**, 527-533.

**Morris, R. L. and Hollenbeck, P. J.** (1995). Axonal transport of mitochondria along microtubules and F-actin in living vertebrate neurons. *J. Cell Biol.* **131**, 1315-1326.

**Nakata, T., Terada, S. and Hirokawa, N.** (1998). Visualization of the dynamics of synaptic vesicle and plasma membrane proteins in living axons. *J. Cell Biol.* **140**, 659-674.

**Neco, P., Gil, A., del Mar Frances, M., Viniegra, S. and Gutierrez, L. M.** (2002). The role of myosin in vesicle transport during bovine chromaffin cell secretion. *Biochem. J.* **368**, 405-413.

**Parton, R. G., Ockleford, C. D. and Critchley, D. R.** (1987). A study of the mechanism of internalisation of tetanus toxin by primary mouse spinal cord cultures. *J. Neurochem.* **49**, 1057-1068.

**Penningroth, S. M., Cheung, A., Bouchard, P., Gagnon, C. and Bardin, C. W.** (1982). Dynein ATPase is inhibited selectively in vitro by erythro-9-[3-2-(hydroxynonyl)]adenine. *Biochem. Biophys. Res. Commun.* **104**, 234-240.

**Prekeris, R. and Terrian, D. M.** (1997). Brain myosin V is a synaptic vesicle-associated motor protein: evidence for a $Ca^{2+}$-dependent interaction with the synaptobrevin-synaptophysin complex. *J. Cell Biol.* **137**, 1589-1601.

**Puls, I., Jonnakuty, C., LaMonte, B. H., Holzbaur, E. L., Tokito, M., Mann, E., Floeter, M. K., Bidus, K., Drayna, D., Oh, S. J. et al.** (2003). Mutant dynactin in motor neuron disease. *Nat. Genet.* **33**, 455-456.

**Rao, M. V., Engle, L. J., Mohan, P. S., Yuan, A., Qiu, D., Cataldo, A., Hassinger, L., Jacobsen, S., Lee, V. M., Andreadis, A. et al.** (2002). Myosin Va binding to neurofilaments is essential for correct myosin Va distribution and transport and neurofilament density. *J. Cell Biol.* **159**, 279-290.

**Reynolds, A. J., Bartlett, S. E. and Hendry, I. A.** (1998). Signalling events regulating the retrograde axonal transport of $^{125}I - \beta$ nerve growth factor in vivo. *Brain Res.* **798**, 67-74.

**Rogers, S. L. and Gelfand, V. I.** (1998). Myosin cooperates with microtubule motors during organelle transport in melanophores. *Curr. Biol.* **8**, 161-164.

**Rogers, S. L. and Gelfand, V. I.** (2000). Membrane trafficking, organelle transport, and the cytoskeleton. *Curr. Opin. Cell Biol.* **12**, 57-62.

**Rose, S. D., Lejen, T., Casaletti, L., Larson, R. E., Pene, T. D. and Trifaro, J. M.** (2003). Myosins II and V in chromaffin cells: myosin V is a chromaffin vesicle molecular motor involved in secretion. *J. Neurochem.* **85**, 287-298.

**Sakowicz, R., Berdelis, M. S., Ray, K., Blackburn, C. L., Hopmann, C., Faulkner, D. J. and Goldstein, L. S.** (1998). A marine natural product inhibitor of kinesin motors. *Science* **280**, 292-295.

**Schiavo, G., Matteoli, M. and Montecucco, C.** (2000). Neurotoxins affecting neuroexocytosis. *Physiol. Rev.* **80**, 717-766.

**Schnapp, B. J. and Reese, T. S.** (1989). Dynein is the motor for retrograde axonal transport of organelles. *Proc. Natl. Acad. Sci. USA* **86**, 1548-1552.

**Tabb, J. S., Molyneaux, B. J., Cohen, D. L., Kuznetsov, S. A. and Langford, G. M.** (1998). Transport of ER vesicles on actin filaments in neurons by myosin V. *J. Cell Sci.* **111**, 3221-3234.

**Tang, F., Kauffman, E. J., Novak, J. L., Nau, J. J., Catlett, N. L. and Weisman, L. S.** (2003). Regulated degradation of a class V myosin receptor directs movement of the yeast vacuole. *Nature* **422**, 87-92.

**Tomishima, M. J., Smith, G. A. and Enquist, L. W.** (2001). Sorting and transport of α-herpesviruses in axons. *Traffic* **2**, 429-436.

**Vale, R. D.** (2003). The molecular motor toolbox for intracellular transport. *Cell* **112**, 467-480.

**Waterman-Storer, C. M., Karki, S. B., Kuznetsov, S. A., Tabb, J. S., Weiss, D. G., Langford, G. M. and Holzbaur, E. L.** (1997). The interaction between cytoplasmic dynein and dynactin is required for fast axonal transport. *Proc. Natl. Acad. Sci. USA* **94**, 12180-12185.

**Wöllert, T., Weiss, D. G., Gerdes, H. H. and Kuznetsov, S. A.** (2002). Activation of myosin V-based motility and F-actin-dependent network formation of endoplasmic reticulum during mitosis. *J. Cell Biol.* **159**, 571-577.

**Wu, X., Bowers, B., Rao, K., Wei, Q. and Hammer, J. A., III** (1998). Visualization of melanosome dynamics within wild-type and dilute melanocytes suggests a paradigm for myosin V function in vivo. *J. Cell Biol.* **143**, 1899-1918.

**Wu, X., Jung, G. and Hammer, J. A., III** (2000). Functions of unconventional myosins. *Curr. Opin. Cell Biol.* **12**, 42-51.